

CHAPTER 109

WAVE-INDUCED BREAKOUT OF HALF-BURIED MARINE PIPES

Mostafa A. Foda¹
Adrian W-K Law²
Jo Y-H Chang²

ABSTRACT

An experimental study is conducted in order to identify the major physical processes leading to the breakout of half-buried submarine pipelines from the seafloor under ocean wave action. Both the hydrodynamic loading on the exposed surface of the pipe, as well as the resulting displacement history of the pipe, were recorded and analyzed in order to identify the critical pipe-soil-wave conditions for the detachment of the pipe from the seabed. The paper also examines the balance of the pipe under the combined lift and drag loading from the water wave. An experimental breakout force-time power law is obtained and compared to available theoretical breakout models.

1. INTRODUCTION

During severe storm or hurricane conditions, wave-induced loading on submarine pipelines can be large enough to detach some of the placed pipes from the sea floor, causing them to move or float to great distances with the ocean currents. Numerous reports of this type of failure to submarine pipes are documented in the literature (e.g. Blumberg 1964, Grace 1978, Christian *et al.* 1974, Nataraja and Gill 1983). With the repeated storm-induced failures of marine pipes, the cost of maintaining their operational integrity can be quite high (e.g. Gerwick 1986). The needed improvement of the cost-effectiveness of the present design and maintenance practice for marine pipelines can clearly be established by gaining more insight into the various processes that constitute the failure mechanism.

This paper aims at studying the mechanical stability of the pipe-soil system under wave action. In particular, we focus on the conditions that lead to pipeline detachment or 'breakout' from the sea floor under hydrodynamic wave loading. We attempt to do that by simulating the breakout process in the laboratory, and further identifying the critical wave-soil-pipe conditions for pipeline breakout. The experimental study is conducted for the configuration of partially buried pipe in a sandy bed under shallow water wave forcing. Partial burial is a commonly observed configuration of submarine pipelines on the sea floor. This may differ from the initial set-up of the pipeline, which may simply be through the direct laying of the pipe on top of the seabed if the water depth is large, or the full or the partial burial of the pipe if the water depth is small. Subsequent interaction between the pipe and the soil will most likely change such initial setting. A marine pipe would then enter into cycles of partial exposure and reburial under the usually variable wave climate conditions. For example, the pipeline may be totally buried initially, but becomes partially

¹Associate Professor, Department of Civil Engineering, University of California, Berkeley, California 94720.

²Graduate Student, Department of Civil Engineering, University of California, Berkeley, California 94720.

exposed due to the erosion of the cover soil by waves. The opposite process of self-burial of the pipe may occur instead due to the erosion of soil particles from underneath the fully-exposed pipe, resulting in the gradual sagging of the pipe into the seabed (e.g. Leeuwestein *et al.* 1985, Hulsbergen 1984, Mao 1986). Another process that results in a partial-burial situation occurs when the pipe is initially laid in an open trench in the seabed. After placing the pipe, local waves and currents at the site will work the spoils back to the artificially-dug trench, leading to a partial-burial configuration.

The first part of this study will focus on the hydrodynamic loading of water waves on partially-buried pipes. This will be done by measuring, in the wave flume, the wave-induced pressure over the exposed surface of the pipe. Then, by integrating the pressure distribution we calculate the resulting forces; drag and lift, and moments on the pipe. Most of the previous studies on wave forcing on submarine pipes were concerned with unburied pipes, with or without close proximity to the seabed (e.g. Sarpakaya 1976, Verley *et al.* 1987). Ismail *et al.* (1986) reviewed the very limited data available on wave loading on partially-buried pipes and stressed the need for detailed measurements of both the hydrodynamic forces as well as the seepage-flow loading on partially-buried marine pipes. In the present study, the measured wave forces will be correlated with wave parameters in order to obtain nondimensional force coefficients for both the drag and lift forces. The widely used Morison Equation will be used to curve-fit the measured drag force on the exposed surface of the pipe, and best-fit coefficients of drag C_D and added mass C_M will be obtained for the range of Keulegan-Carpenter numbers of our experimental set-up. A nondimensional lift-force coefficient C_L will be obtained following a similar procedure.

Then, the study will concentrate on the response of the pipe-sand system to the applied wave forcing. In particular, we examine how will the pipe react to the applied forcing, and how does the detachment process take place. Earlier body breakout studies were concerned with the detachment process under constant applied lift force (e.g. Liu 1969, Muga 1969, DeHart and Ursell 1967). A complete detachment was observed to take place only after the lift force has been applied for a certain period of time, normally called 'the breakout time'. The process is usually very slow in the beginning, concluded by a rather sharp release at the breakout time. It was concluded that this almost yield-type release is related to the strong coupling between the body and the saturated bed. Foda (1982, 1983) developed a theory that describes the quasistatic detachment of a large semiburied object from a poroelastic bed. In the theory, this initial resistance to body movement is attributed to the development of negative pore-pressure, or 'mud-suction' at the body-soil interface, which gives rise to a certain seabed holding strength against body breakout. The nature of this mud-suction resistance can be illustrated by considering the behavior at the body-soil interface. Initially, as the body moves upward in response to the applied lift force, some pore water will have to be moved, or sucked, upward in order to fill in the resulting gap between the body and the soil. Such movement of pore water requires pore-pressure gradient in order to push the flow through the pores against viscous resistance stresses (Darcy's law), giving rise to the negative pore-pressure at the body-soil gap. The yield-type release will occur late into the lift-off process, when the body-soil gap is wide enough to allow ambient water from above the bed to flow laterally into the gap through its periphery. The resistance to such lateral flow into the gap is far less than that for the upward pumping of pore water into the gap, and at this stage there is virtually no resistance to the further expansion of the body-soil gap, and hence the quick release. The analysis resulted in a general breakout time-force power law of the form:

$$F_b = C t_b^{-n} \quad ; \quad n = 1.5 \quad (1)$$

where t_b is the breakout time, F_b is the breakout force, or the applied lift force in excess of the submerged weight of the body, and C is a material constant that depends on the permeability, stiffness and porosity of the saturated bed, as well as the size of the body (Foda 1983). However, the above law is limited to the conditions of the boundary-layer

theory of Mei and Foda (1981), which requires that the pipe diameter D is much larger than the seabed boundary-layer thickness δ which is roughly proportional to $\sqrt{k/\mu\omega}$ where k is the soil permeability, μ is water viscosity, and ω is wave frequency. Mei *et al.* (1985) developed another breakout law for bodies on a porous but rigid bed that has the same form as (1), but with a different material constant C and power n ($n = 1$). This law would be more applicable to pipes with a small enough diameter.

Foda (1985) extended his theory to the present case of a half-buried marine pipe under the oscillatory loading of water waves. The hydrodynamic loading on the pipe is calculated assuming a potential flow above the seabed. Furthermore, it was assumed that the pipe diameter D is much smaller than both the wave length L and the water depth h , so that wave scattering by the pipe was ignored. Only the vertical equilibrium of the pipeline was considered under the wave-induced lifting force, which is composed in this case of an average lift force plus an oscillatory component. The analysis has shown that for typical physical parameters, the wave period $T \approx 10$ sec is usually much shorter than the quasistatic breakout time t_b , and hence one expects that the oscillatory wave-induced force component will not influence, to leading order, the breakout process of the pipe.

The possibility of resonating the system by the oscillatory force was also examined. The obtained response function of the pipe-seabed system was shown to exhibit a weak nonlinearity of the order $\epsilon = T/t_b \ll 1$. This should lead to the slow generation of higher harmonics and hence raises the possibility of resonating the system when one of the generated harmonics approaches the system's natural frequency. However, the analysis has shown that the natural frequency of a 'typical' pipe-soil system would be much higher than water wave frequency, so that a long chain of generated higher harmonics would be needed in order to approach the resonance condition.

The present experimental study examines many of the features of the above mentioned breakout models, along with the associated assumptions and limitations. This includes investigating the nature of the pipe breakout (quasistatic or resonant), the relative role of pore-pressure vs. soil effective stresses in holding the pipe in place, and the ultimate mode of failure for the supporting soil at breakout.

2. EXPERIMENTAL SETUP

The experimental work was conducted in the 8 ft (W) \times 5 ft (H) \times 180 ft (L) wave flume at the Richmond Field Station of the University of California at Berkeley. The relatively large cross-sectional area of the flume allowed the building of a reasonable-size sand basin inside the flume to model the seabed. A layout of the experimental setup is shown in Figure 1a. The flume is fitted at one end with a mechanical flap-type wave maker that generates monochromatic water waves, with a range of possible wave amplitudes and frequencies. At the other end of the flume, a 20° sloping beach with four layers of horse-hair mats is built to absorb the incoming wave energy. The test section is built about 50 ft from the wave maker where there is a side-viewing glass window in the flume's concrete wall. As shown in Figure 1, the test section is made of a rectangular sand basin 2 ft high, 8 ft wide and 4.5 ft long. Two 20°-plywood ramps are fitted at both ends of the basin in order to provide smooth transitions for the water wave as it passes over the test section. The sand used in the experiments was a well sorted medium-size sand of $D_{50} = 0.3$ mm. The basin was filled with the sand, manually compacted in the dry, then an 8" PVC pipe was placed across the flume, half-buried in the sand bed. The length of the pipe was cut slightly shorter than the width of the flume (8 ft) to prevent friction between the pipe and the flume's concrete walls. The pipe would then be connected to the various sensors of the experiment, feeding into a data-acquisition system whose details are discussed in the following section. Then, the flume would be filled with water to a total depth of 4 ft (2 ft of water above the sand bed).

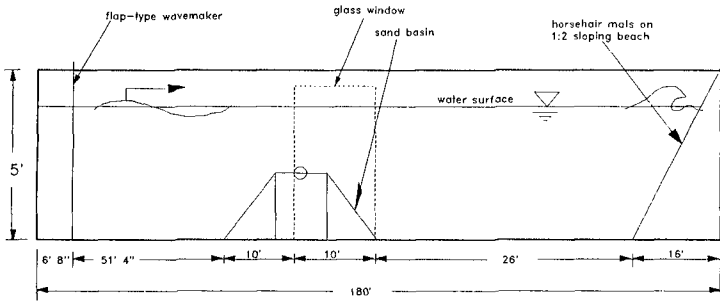


Figure 1a: A sketch of the flume dimensions

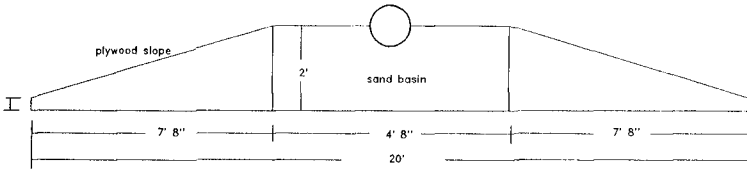


Figure 1b: The sand basin dimensions

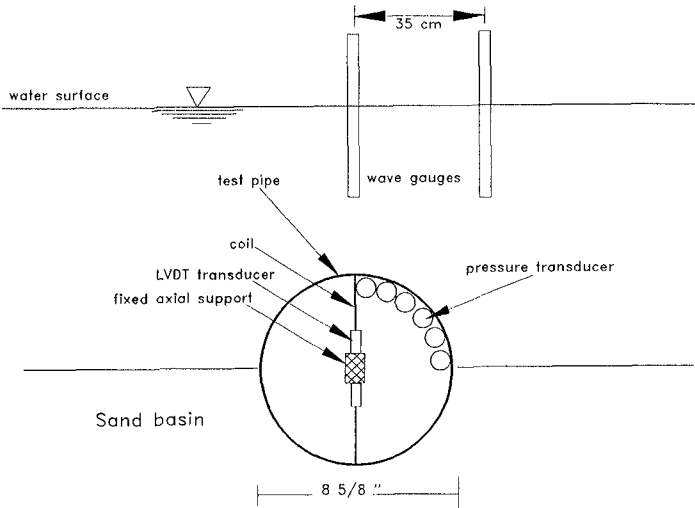


Figure 2: Experimental Setup

A typical experimental run would start by turning on the motor of the wave maker to generate a monochromatic wave of pre-set wave height and frequency (typically, 6" and 3 sec, respectively), and continuously recording the measurement data on water pressure around the pipe, pore pressure measurements, wave profile above and near the pipe, and the displacement history of the pipe, until failure, or detachment, of the pipe from the sand bed occurs (or until termination of the run if breakout does not occur). In many runs, the whole test section would be videotaped to record the visible behavior of the pipe-soil system throughout the experiment.

3. DATA-ACQUISITION SYSTEM:

In order to measure the wave-induced hydrodynamic loading on the pipe a total of six pressure transducers (Data Instrument Model AB High Performance 0-6 psi) was used to measure pressure distribution over one quarter of the exposed pipe surface (Figure 2). The pipe would simply be rotated 90° to measure water pressure over the other quarter surface. The pressure transducers were placed inside the 8"-pipe at the midlength section. The transducers were connected to the outside of the pipe through an array of small holes 15-degrees apart drilled through one quarter of the pipe's wall. Small plastic tubings (1/8" inner diameter, 4" long) were used to connect these holes to the diaphragm-type pressure transducers. The output signals from the transducers were then amplified by accurate strain gauge conditioners (Daytronic 9178A), enhancing the resolution to about $1 N/m^2$. Although this accuracy is over the manufacturer recommended limit (0.25% of full range), calibration of the transducers showed a repeatable linear curve with constant slope, indicating that the extrapolation of accuracy is valid.

The measurement of pore-pressure, or mud-suction stress, along the pipe-soil interface was made following the same procedure by rotating the pipe so that the measurement holes would be on the buried half of the pipe surface.

As for the movement of the pipe, two Linear Variable Differential Transformers, LVDT, were used to measure both the vertical and the horizontal components of the pipe's displacement. Since the pipe was totally immersed into water, a hermitically-sealed type was selected (Schaevitz 500HPA). The selected LVDT has a measurement range of about one inch and an accuracy of 1/4000 of an inch using an analog transducer amplifier (ATA101) from the same company. The magnetic coils of the two LVDTs were mounted on an aluminum frame that runs through the center of the pipe, with its ends fixed on the side walls of the wave flume (Figure 2). One coil is mounted in a vertical orientation, while the other is mounted horizontally, normal to the axis of the pipe. The metallic center rods of the LVDTs were then placed through, but not touching, their respective magnetic coils and attached to the the pipe's interior wall. In this arrangement, both the vertical and the horizontal displacement of the pipe can be measured by detecting the relative motion between the coil and the center rod of each LVDT, without restraining the free motion of the pipe under wave loading.

The wave profile is measured by using two double-wire wave gauges which relate changes in resistance and hence voltage of the partially-immersed wires with changes in water level. The accuracy of the recorded water level was about 0.3 mm with careful calibration. One wave gauge was located directly above the pipe and the other was about 35 cm downwave towards the dissipative beach. The gauges were isolated electronically to avoid possible interference and together they measured the wave profile at the test section and also the amount of reflection from the beach. They are excited and their signals amplified by strain gauge conditioners (Daytronic 9178A) similar to those used for the pressure transducers.

The data-processing unit was an IBM PC/AT equipped with two data acquisition cards (IBM Data Adapter and Datatranslation Data Board DT2801). This provides for 12 channels

with 12-bit accuracy. A program is written in C-language to allow the start or termination of the recording of any signal at any time during the experiment independently or synchronically with other signals. In addition, during the recording, the program can still report values of any desired signal. These features add more flexibility on memory storage and early detection of errors.

4. THE BREAKOUT EXPERIMENT:

In all of the conducted experiments, the observed behavior was very similar, consisting primarily of two distinct phases. First, there is the build-up phase, which covers more than 90% of the duration of the experiment. Then, there is the short phase of actual pipe-breakout from the sand bed. During the build-up phase, there is hardly any discernible movement of the half-buried pipe. The only visible movement was that of some of the sand grains on the surface of the sand bed, which quickly resulted in the establishment of a regular ripple pattern on both sides of the pipe. However, in the near proximity of the pipe (about one pipe diameter distance on either side), no motion of sand grains was visible and the sand surface there remained flat throughout this phase. In other words, one can say that in our set-up soil erosion did not play any role in the ensuing behavior of the pipe-sand system.

The duration of this build-up phase ranged from about half an hour to a little less than 5 minutes. During this phase, the pipe was clearly subjected to the hydrodynamic lift and drag due to the passing of water waves above it. Flow separation was observed to take place in all the experiments. Separation was made visible by injecting liquid dye near the exposed surface of the pipe. The dye would quickly encounter and make visible one or more of the shedded vortices from the surface of the pipe. Such viscous separation would result in an asymmetric distribution of pressure around the pipe, and hence a net loading on it. Another cause for pressure asymmetry is the added-mass effect associated with the unsteadiness of the flow. Furthermore, there is the lift-force component associated with the Bernoulli's effect, where the increase in velocity at the summit of the pipe is accompanied by a decrease in pressure, i.e. a lift. The details of the measured hydrodynamic loading on the pipe will be given in the following Section.

By examining the displacement record of the pipe during this initial build-up phase, we observe that the response of the pipe to these applied hydrodynamic loadings is in the form of a very small oscillatory motion, with a very slow net movement in the upward direction. Figure 3 shows the vertical displacement history of the pipe center during a typical run. In this Figure, the amplitude of the pipe oscillation is about .008 inch, and the average rate of rise of the pipe during this build-up phase is of the order of .10 inch/minute, which can hardly be detected by the naked eye. Superimposed on this gradual rise, there was an even slower rotational movement of the pipe around its longitudinal axis. This suggests that the pipe is actually rolling out of the sand bed, as opposed to being uniformly lifted off from the bed. With the wave coming from left-to-right the observed net rotation was always anticlockwise. In other words, the combined rise and roll motion of the pipe did have an effective pivot point (point of zero net displacement) which was always at the wave-maker side from the pipe center. The rotational displacement was measured by placing markers at equal distances on the pipe wall and visually recording the difference between the reading at the two pipe-soil contact lines. This would typically reach a maximum value, at pipe breakout, of about 10-15 degrees.

It is important to note that throughout this phase where the pipe is slowly building up towards the ultimate breakout, the soil mass surrounding the pipe remained intact, with no sign of any soil failure, such as soil sliding, erosion or soil liquefaction. Finally, near the end of this build-up phase, the pulsating motion of the pipe becomes easier to detect by the naked eye, and this signals the start of the very short second phase of pipe breakout.

As seen in Figure 3, the very slow, almost unnoticeable rise of the pipe during this long build-up phase is followed by the rather sudden and violent release of the pipe from the sand bed in the breakout phase. The release is so sudden that it is relatively easy to identify a specific time when that happens, and we may term that the 'breakout time'. From Figure 3 we see that approaching the breakout time there is no significant increase in the amplitude of the oscillatory motion, and that the breakout is essentially associated with the increase in the net rise component of the motion. This should quite reasonably exclude resonance as the possible mechanism for such a breakout. Instead, it is a quasistatic process through which the pipe gradually detaches itself from the sand bed, against the so-called 'mud-suction' resistance force. The eventual breakout occurs due to the dissipation of this mud-suction force at breakout time. The details of the breakout mechanism will be discussed later in this paper. But first, we discuss the hydrodynamic loading that forces such breakout.

5. HYDRODYNAMIC LOADING:

Figure 4 shows the distribution of dynamic water pressure on the exposed half-surface of the pipe during one wave cycle (wave period of 2.9 seconds and wave height of 6"). This is obtained by combining two 1/4-surface data, under identical wave profiles. For any point on the exposed pipe surface, it is seen that pressure is nearly in-phase with the wave profile, i.e., the maximum and minimum pressure occur almost under the crest and trough of the wave, respectively. From the Figure, it is seen also that under either the crest or the trough, the pressure distribution has a minimum near the summit of the pipe (near points 6 and 7), where the kinetic energy is a maximum due to the pipe-induced contraction of the flow, (the Bernoulli's effect). This will clearly result in a net lift force on the pipe. Aside from that, there is some asymmetry in crest and trough pressure distribution around the summit point. This may be attributed to flow separation effect. A more pronounced asymmetric distribution of pressure is however due to the added-mass effect and is evident in the Figure near the wave's nodal points (time = 1.0 s and 2.0 s), where flow acceleration is maximum. This asymmetry and the resulting loading on the pipe are due to the pipe-induced deceleration of a certain amount of fluid mass in the pipe's vicinity.

By integrating the measured pressure distribution over the pipe surface, the wave-induced drag and lift can be found. Figure (5) shows sample results for the measured drag force on the half-buried pipe. The Figure also shows the least-square fitting of the data in the form of a Morison Equation:

$$F_D = \frac{1}{2} C_D \rho(D/2) u|u| + C_M \rho(\pi D^2/2) \frac{du}{dt} \quad (2)$$

where $u(t)$ is the unsteady ambient water velocity near the pipe, D is the pipe diameter, ρ is the water density, C_D is the drag coefficient, C_M is the added-mass coefficient. The ambient water velocity was estimated using Dean's stream-function calculation. First, the stream-function was tuned to reproduce the measured water surface elevation $\eta(t)$, and then the corresponding bottom water velocity was calculated. Figure 6 shows a sample of the calculated bottom velocity for a measured $\eta(t)$. Over many selected wave cycles, the best-fit values for the drag coefficient ranged between -0.188 to +0.861, while the added-mass coefficient ranged from 1.51-2.08. From potential theory, assuming no flow-separation, the added-mass coefficient (which should be the same for either a half or a full cylinder) is predicted to have a value of 2 (Lamb 1932). For real fluids, the values of C_M and C_D would depend on the Keulegan-Carpenter Number $U_0 T/D$, where U_0 is the amplitude of the velocity oscillation, T is the wave period, as well as on Reynolds Number $U_0 D/\nu$, where ν is the kinematic viscosity (e.g. see Sarpakaya 1976 for full cylinders near flat bed). In our experiments, the Keulegan-Carpenter Number was around the value of 6, and the Reynolds Number was in the order of $(0.8 - 1.0) \times 10^6$.

PIPE DISPLACEMENT HISTORY

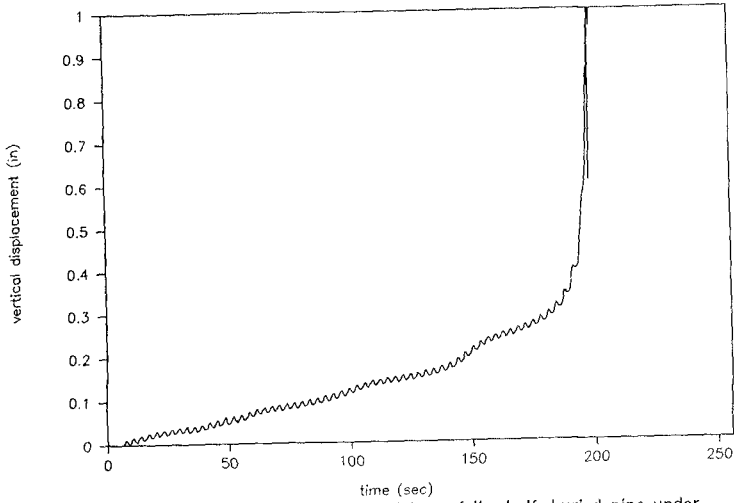


Figure 3: Vertical displacement history of the half-buried pipe under 6"-2.9sec water wave

PRESSURE DISTRIBUTION

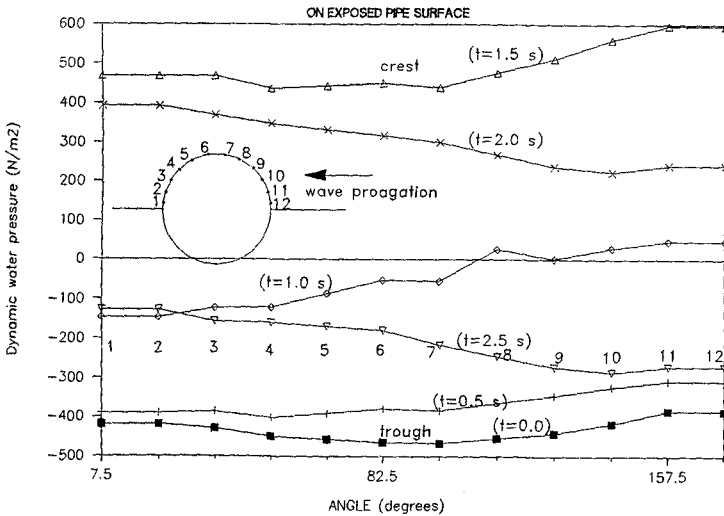


Figure 4: Measured water pressure on the exposed half-surface of the pipe over one full wave cycle (wave height 6", wave period 2.9 sec).

HYDRODYNAMIC DRAG ON THE HALF-PIPE

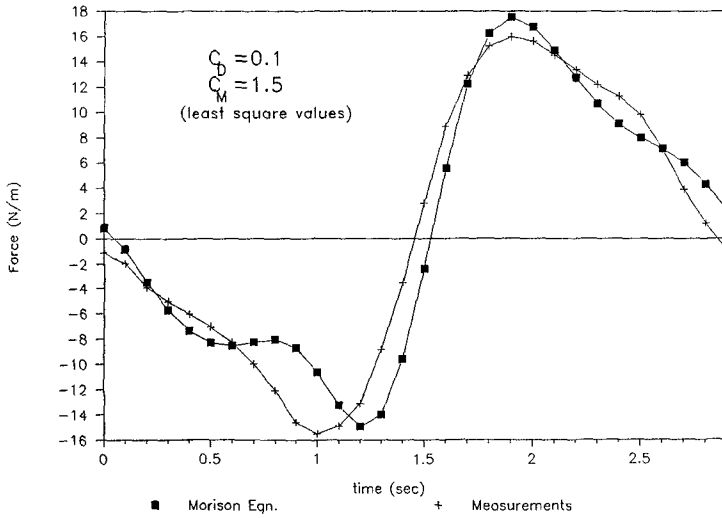


Figure 5: Curve fitting the measured drag force on the half-surface of the pipe with Morison Equation.

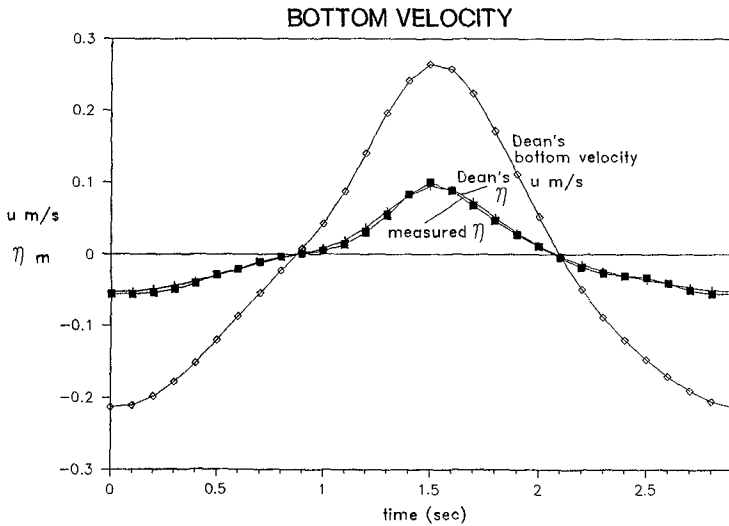


Figure 6: Comparison between measured vs. predicted water wave profile, and the resulting bottom velocity u using Dean's stream function.

As for the lift force F_L , we used the following expression to curve-fit the data

$$F_L = \frac{1}{2} C_L \rho D u^2 \quad (3)$$

where C_L is the nondimensional lift coefficient. The best-fit value for C_L , averaged over many wave cycles, was found to be 2.556, which is close to the theoretical value of 2.66 from potential flow theory (e.g. Milne-Thomson 1967).

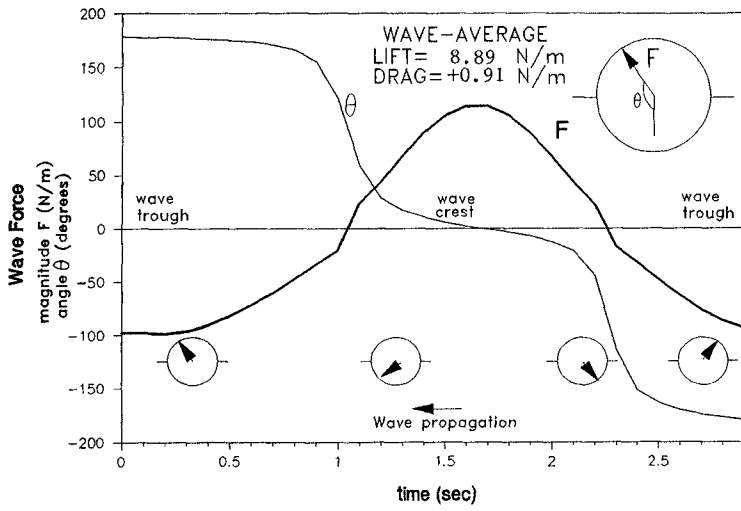
Figure 7 shows sample results for the measured resultant hydrodynamic force on the pipe during one wave cycle. Notice that the resultant pressure force is passing, by definition, through the center of the pipe. With the wave propagating from right-to-left, the resultant force is rotating in an anticlockwise sense with a non-constant angular velocity, as is seen from the variation of the force angle θ with time. Clearly, the average angular velocity of the resultant force is equal to the wave frequency ω , but as seen from $\theta(t)$, the resultant force tends to slow down (below ω) when the force is near vertical, upward or downward, with a fast transition (above ω) between them. Notice also that the wave average drag and lift forces are much smaller than the respective amplitudes of the oscillatory forces. The wave-average lift is always directed upward, and its magnitude is found to be very close to the potential theory calculation, i.e., by wave-averaging (3) with $C_L = 2.66$. However, the far smaller net drag is observed to fluctuate in magnitude and even in direction; sometimes in the wave direction (Fig 7a) and sometimes opposite to the wave direction (Fig 7b).

6. THE BREAKOUT MECHANISM:

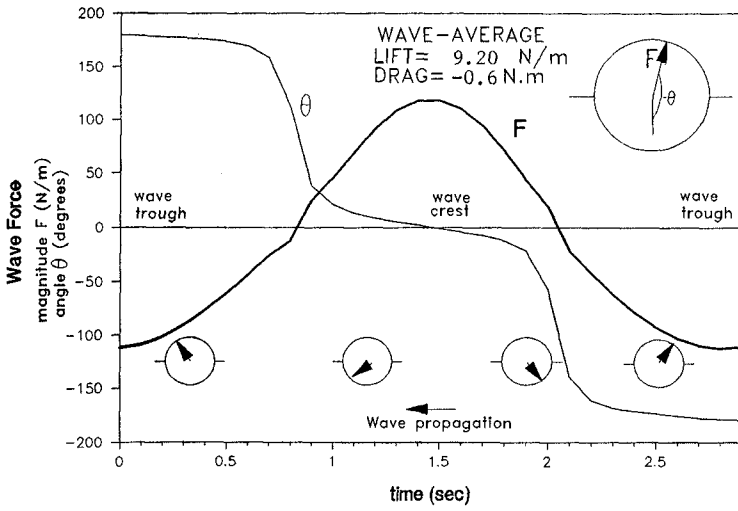
If the wave-averaged lift force exceeds the buoyant weight of the pipe, then the pipe will try to move upward in response. This will initiate two types of resistance forces along the pipe-sand interface, both acting to keep the pipe in place. One is the shear stress between the pipe and the sand grains, and the other is the negative pressure in the pore water below. That negative pore-pressure would be developed as some pore water will be forced to move upward along with the upward-moving pipe. For typical, low-permeability soils, the developed negative pore-pressure can be quite appreciable even for a very slight initial motion of the pipe. For example, a 1-m diameter pipe with an initial motion of only one hundredth of an inch above a fine-sand bed (permeability $k = 10^{-12} \text{ m}^2$) will produce, according to Darcy's law, a negative pore-pressure impact force of the order of 10^5 N-s/m . On the other hand, the value of the sand shear stress has an upper limit given by the relatively low Coulomb sliding shear for this unconfined, near-surface sand around the pipe.

The rate of vertical movement of the pipe will depend on the rate of water penetration into the developing gap between the pipe and the soil below. This water penetration can come from two possible sources: (a) the seepage flow of water into the gap across the soil surface, and this depends on the soil properties, especially its permeability and stiffness, and (b) the ambient water flow above the seabed through the gap periphery, which according to the lubrication theory is proportional to the gap thickness to the third power. In the initial stages of lift-off, the gap thickness is very small and thus its expansion will be essentially due to the penetration of pore water through the soil matrix. Since the pore water flow through the soil is typically very slow (governed by soil permeability), the pipe lift-off velocity during this stage will be very small (see Fig 3). With time, the gap thickness becomes large enough so that the lateral flux of ambient water through the gap periphery gains dominance over the pore water flux. As a result, the resistance to further gap expansion becomes much smaller than the pull-up force (e.g. lubrication theory), and hence the quick release at breakout time.

This is the basis of the theoretical breakout model of Foda (1985). In reality, however, there are a number of other factors that may be contributing to the breakout process, but are



(a)



(b)

Figure 7: The variation of the total wave force magnitude and direction over two selected wave cycles.

not considered in this idealized model of Foda. For example, there is the question of the role of wave-induced drag force during the breakout process. In the above discussion, we focused on the response due to the applied lift force, which if acting alone on the pipe would result in a uniform lift-off of the pipe away from the underlying soil. However, in reality, the pipe is responding to the combination of lift and drag forcings. Furthermore, the model assumes that the pipe resistance against breakout is entirely provided by the negative pore-pressure or mud-suction stress at the pipe buried surface. In general, however, there will be some direct contact between the pipe surface and the sand solid skeleton, and hence there is the combination of pore pressure and effective (solid) soil stress that will be acting there, and it is of interest to compare the relative magnitudes of the solid vs. pore-fluid stresses that are actually acting on the buried pipe surface.

By integrating the pressure over either the upper, exposed surface l_e , or the lower, buried surface l_b , we get the corresponding fluid loadings on the pipe as follows:

$$(F_L, F_D)_{h,p} = \int_{l_e, l_b} p(\theta, t) (\sin \theta, \cos \theta) d\theta \tag{5}^\dagger$$

where F_{Lh}, F_{Dh} are the hydrodynamic lift and drag forces, and F_{Lp}, F_{Dp} are the pore-water lift and drag forces, respectively. It is further seen from Figure 4 that the pipe displacement is very small so that we may invoke the static balance equations in both the horizontal and vertical directions:

$$F_{Dh}(t) = -[F_{Dp}(t) + F_{Ds}(t)] \tag{6a}$$

$$F_{Lh}(t) = -[W + F_{Lp}(t) + F_{Ls}(t)] \tag{6b}$$

where F_{Ls} and F_{Ds} are the remaining soil lift and drag forces on the pipe due to the direct contact between the pipe and the soil's solid skeleton, and W is the submerged weight per unit length of the pipe.

A Fast Fourier Transform (FFT) is performed on Equations 6a,b in order to separate out the balances at the wave-averaged or zeroth-harmonic mode from the first and higher harmonic balances. The results for the fluid loadings are shown in Figures 8a,b. The discrete Fourier transform is defined as:

$$\overline{F}(m, \Delta\omega) = \frac{T_0}{N} \sum_{n=0}^{N-1} F(n, \Delta t) e^{-i2\pi mn/N}; \quad m=0,1,\dots,N/2 \tag{7}$$

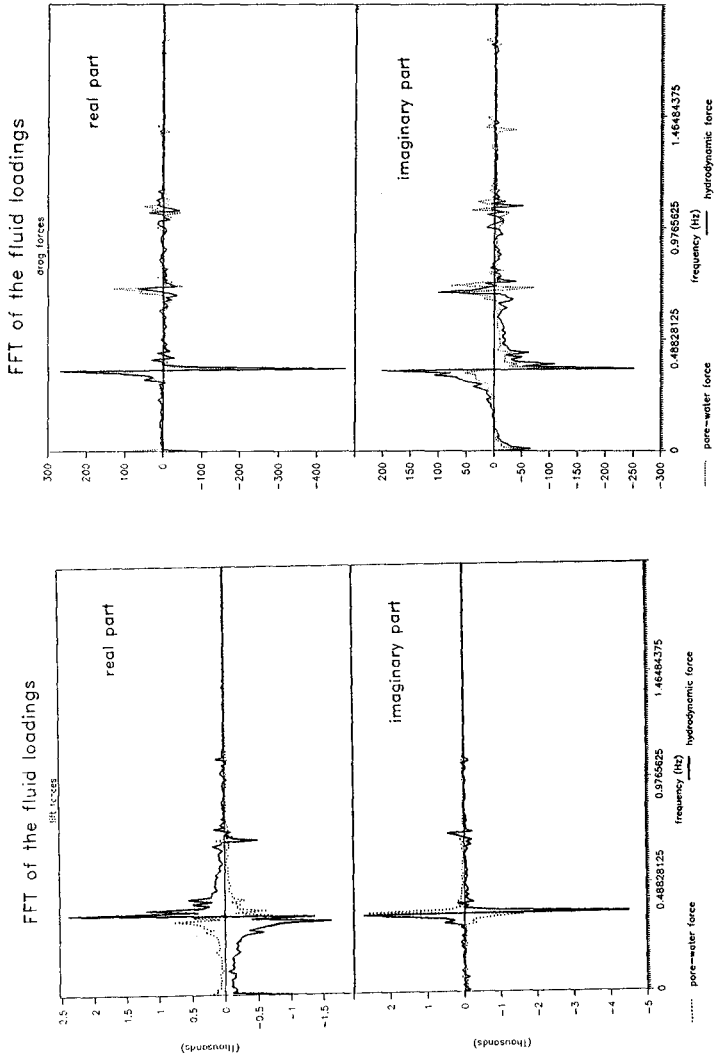
where the overbar denotes the Fourier transform, Δt is the sampling time increment which is taken here to be equal to 0.1 sec, N is the total number of data points, $T_0=N\Delta t$ is the duration of sampling, taken equal to 102.4 sec, and the incremental frequency $\Delta\omega=2\pi/T_0$. The results in Figures 8a,b correspond to the initial period (i.e. the first 102.4 s) of a selected breakout experiment with the same conditions as those for Figure 4.

Let us first examine the zeroth-harmonic ($m=0$) vertical response, which requires from (6b) that,

$$\overline{F}_{Lh}(0) / T_0 = - [W + (\overline{F}_{Lp}(0) + \overline{F}_{Ls}(0)) / T_0] \tag{8}$$

By accurately measuring the dry weight of the pipe and subtracting the water buoyancy we obtained a value of $W = 7.796 \text{ N/m}$. Furthermore, as seen from Figure 8a, we find that the

[†]Equation (4) is missing due to an error in numbering the equations.



(a)

(b)

Figure 8: The Fast Fourier Transform of the hydrodynamic (solid lines) and pore-water (dotted lines) loadings on the half-buried pipe; (a) lift forces, (b) drag forces.

wave averaged hydrodynamic lift $-\overline{F}_{Lh}(0)/T_a$ is equal to $1021.8/102.4 = 9.98 \text{ N/m}$, while the wave-averaged pore-water suction force $F_{Lp}(0)/T_a$ is equal to $230.8/102.4 = 2.25 \text{ N/m}$, which virtually satisfies the vertical balance in (8) with negligible contribution from the soil effective stress forcing on the pipe; a mere -0.066 N/m according to (8). Turning to the zeroth-harmonic horizontal balance (see Figure 8b), we find a steady-state hydrodynamic drag on the pipe of a magnitude of 0.73 N/m , in the direction of wave propagation. We also find that the steady-state pore-water reaction force is equal to 0.817 N/m acting in the opposite direction. Again, there is an almost complete balance between the hydrodynamic and pore-water forces, with only a small contribution from the soil effective-stress loading, equal to the difference 0.087 N/m . It is curious, however, to note that these small soil loadings in both the horizontal and vertical directions are acting in the same direction as the the forcing hydrodynamic loadings. A partial explanation of this observation will be offered shortly.

We turn next to examine the balance of forces at the primary first harmonic, @ the wavemaker frequency $1/T = 0.345 \text{ Hz}$; $T = 2.9 \text{ sec}$. First, from Figure 8a we see that there is a 180° phase-shift between the hydrodynamic and pore-water vertical loadings almost throughout the frequency spectrum. But, we also see that the pore-water vertical force balances out only a proportion α of the forcing hydrodynamic loading, i.e.

$$\overline{F}_{Lp} = -\alpha \overline{F}_{Lh} \quad (9)$$

Except for a few very low frequencies near $m=0$ (giving higher values for α), the value of α is found to be relatively constant around $\alpha = 0.55$. That is to say that roughly 55% of the total soil reaction force to the unsteady hydrodynamic lift on the pipe is taken up by the pore-pressure. The remaining 45% of the soil reaction has to come from the soil-effective stress loading on the pipe. This contrasts drastically with the above-mentioned steady-state ($m=0$) results, where there is negligible effective stress contribution to the balance of forces.

The role of effective stresses is even more prominent in the horizontal forces balance. From Figure 8b it is seen that the unsteady ($m \neq 0$) hydrodynamic and pore-water drag forces on the pipe are in fact in-phase. This means that the pore-water unsteady drag is reinforcing, not balancing, the hydrodynamic unsteady drag. Therefore, it is the role of the soil solid skeleton to provide the effective stress loading necessary to balance the combined fluid drag force (hydrodynamic + pore-water). On the other hand, it should be noted that even this combined fluid drag on the pipe is an order of magnitude smaller than the hydrodynamic lift, as can be seen by comparing the ordinate scales in Figures 8a vs. 8b. Furthermore, we note that the drag-induced effective stress is not additive to the lift-induced effective stress, since they are almost 90° out-of-phase. This is evident from Figures 8a,b where we have two almost real lift spectra, and two almost imaginary drag spectra. It is also a consequence of the dominance of the added-mass drag component, as discussed before and as evident in Figure 5.

From the above, we may conclude that the pipe is in constant contact with the underlying soil, and the resulting effective stress loading on the pipe is, in part, balancing a proportion (~45%) of the wave lift force, and in part balancing the total fluid drag on the pipe. The elastic pipe displacement should be in-phase with the effective-stress loading, and thus should follow the same pattern as that of the force F in Figure 7, with a resulting anticlockwise orbital path of the pipe center over one wave cycle.

Superimposed on this oscillatory motion, there is the zeroth-harmonic response due to wave-averaged lift and drag forces. As predicted by Foda (1985), this response is entirely in the form of a mud-suction force or negative pore-pressure along the pipe-soil interface. The resulting motion is a gradual lift-off of the pipe as shown in Figure 3. The much smaller steady-state drag force is causing a slight antisymmetry in the mud-suction stresses and hence a very small deviation from the uniform lift-off condition. In other words, the

slow pipe motion will have both a net vertical upward component as well as a much smaller horizontal component in the same direction as the fluid drag, i.e. in the direction of wave propagation.

Next, we briefly discuss some of the possible dynamic interaction between the first and zeroth harmonic responses (e.g. Foda 1985). In particular, we heuristically discuss one specific possibility, namely, the role of the first-harmonic drag force on the net, or zeroth-harmonic pipe motion. First, we note that due to the oscillatory fluid drag, the pipe will be bouncing back-and-forth against the sides of the soil circular interface. The problem can be modelled as a simple elastic bouncing of a body off an elastic surface with an oblique impact angle. Therefore, as the pipe impacts on this nonvertical soil surface it will clearly bounce back from the surface acquiring a small additional vertical velocity in the upward direction. This is because the elastic strains in the soil due to this horizontal pipe impact will include vertical compressional strains along the circular soil interface. This small upward bounce, or roll-out, due to wave drag would clearly occur regardless of the direction of the drag. Therefore, there should be a net, or a wave-averaged (zeroth-harmonic) upward motion, as well as an upward effective-stress force on the pipe due to such mechanism. An indication of such upward effective-stress force was observed above when considering the balance of forces according to Equation (8). However, the obtained magnitude of this force, from the analysis that follows Equation (8), is seen to be negligibly small so that, at least in our case, such roll-out mode of motion is deemed to be of little significance to the total breakout process.

Finally, Figure 9 shows the experimentally obtained data on the breakout force-time relation. The breakout force F_b is defined here as the net uplift force acting on the pipe, which is given by

$$F_b = \bar{F}_{Lh}(0)/T_0 - W \quad (10)$$

and the breakout time t_b is determined from the recorded displacement histories (similar to Figure 4) when the slope of the curve reaches 90% of vertical. The best-fit power law that runs through the experimental data was obtained using a least-square routine, and is given in SI-units by

$$t_b = A F_b^{-0.93} ; A = 1477 \quad (11)$$

The exponent is very close to Mei *et al.* (1985) power law for breakout of flat-bottomed bodies from a porous rigid bed. Their law is given by

$$t_b = \tau(\mu L^{7/3} k^{-2/3}) F_b^{-1} \quad (12)$$

where μ is the water viscosity, k is the soil permeability, L is contact width of the two-dimensional body, and τ is a nondimensional coefficient that ranges between 0.4-0.62 depending on the assumed slip boundary condition at the bed surface. Using conformal mapping, the above analytical relation was extended to our configuration of a half-buried pipe and the details are given in Law *et al.* (1988). The result is a modification in the value of τ from that for flat-bottomed bodies. For example, for a no-slip boundary condition at the bed surface, we get

$$\tau = 1.9 \quad (13)$$

The increase in the value of τ , and hence the breakout time t_b , is due to the nonuniform shape of the resulting gap between the pipe and the bed, with the smallest gap thickness being at the gap periphery. This will clearly reduce the lateral flux of ambient water through the gap periphery, as compared to the case of a flat-bottomed body, and hence delay the breakout time.

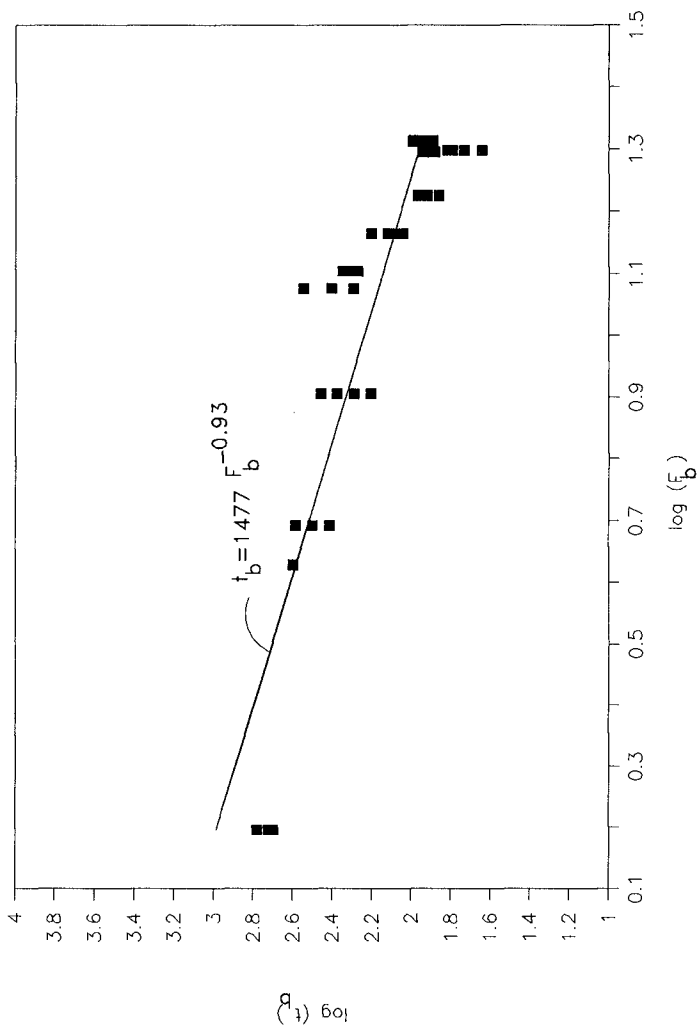


Figure 9: The experimentally-obtained breakout force-time relation

Now, recasting the constant coefficient A in (11) to be of the form of the material constant of the law in (12), where $\mu = 10^{-3} \text{ kg/m-s}$, $k = 0.32 \times 10^{-10} \text{ m}^2$ (measured using a constant head permeometer), $L = \pi D/2$, and $D = 0.2191 \text{ m}$, we find that the corresponding value of the free parameter τ is equal to

$$\tau_{\text{exp}} = 1.78 \quad (14)$$

which is very close to the theoretical value in (13).

ACKNOWLEDGMENTS

This research was sponsored by NOAA, National Sea Grant College Program, Department of Commerce, under grant number NA85AA-D-SG140, project number R/OE-2, through the California Sea Grant College Program.

REFERENCES

- Blumberg, R., "Hurricane winds, waves and currents test, marine pipeline design," Pipeline Industry, June-Nov. 1964.
- Christian, J.T., Taylor, P.K., Yen, J.K. and Erali, D.R., "Large diameter underwater pipeline for nuclear power plant designed against soil liquefaction," Offshore Technology Conference Proc., 2, 597-602, 1974.
- DeHart, R.S. and Ursell, C.R., Southwest Research Institute Report on Contract N-ONR-336300, 1967.
- Foda, M.A. "On the extrication of large objects from the ocean bottom, the breakout phenomenon," J. Fluid Mechanics, 117, 211-231, 1982.
- Foda, M.A. "Breakout theory for offshore structures seated on seabed," Proc. Specialty Conf. Geotech. Practice In Offshore Engineering, 288-299, Austin-TX, ASCE 1983.
- Foda, M.A. "Pipeline breakout from seafloor under wave action," Applied Ocean Research, Vol 7(2), 79-84, 1985.
- Gerwick, B.C.Jr. "Construction of Offshore Structures," New York: Wiley, 1986.
- Grace, R.A. "Marine Outfall Systems: Planning, Design and Construction," New Jersey: Prentice-Hall 1978.
- Husbergen, C.J. "Stimulated self-burial of submarine pipelines," OTC-2967, Houston-TX, May 1984.
- Ismail, N.M., Wallace, N.R. and Nielsen, R., " Wave forces on partially buried submarine pipelines," OTC-5285, 27-36, Houston-TX, May 1986.
- Law, A. and Foda, M.A., "Breakout of half-buried pipe from a rigid porous bed," Technical Report HEL- (in-press), University of California, Berkeley, 1988.
- Leeuwestein, N., Bijker, E.W., Peerbolte, E.B. and Wind, H.G., "The natural self-burial of submarine pipelines," BOSS'85, Delft July 1985, Amsterdam: Elsevier, Dev. Mar. Technol., Vol.2, Paper C18, 717-728, 1985.

Liu, C.L., "Ocean sediment holding strength against body breakout," U.S. Naval Civil Eng. Lab., Port Hueneme-CA, Tech. Rep. R635, 1969.

Mao, Y., "The interaction of a pipeline with an erodible bed," Institute of Hydrodynamics and Hydraulic Engineering, Technical University of Denmark, Research Series Paper No. 39, 1986.

Mei, C.C., Yeung, R.W. and Liu, K.P., "Lifting of a large body from a porous seabed," J. Fluid Mechanics, 152, 203-215, 1985.

Mei, C.C. and Foda, M.A., "Wave-induced response in a fluid-filled poro-elastic solid with a free surface - A boundary-layer theory," Geophy. J. R. Astro. Soc., 66, 597-637, 1981.

Milne-Thomson, M.N. "Theoretical Hydrodynamics," 5th ed., New York:MacMillan.

Muga, B.J., "Ocean bottom breakout forces, including field test data and the development of an analytical method, Tech. Rep. R591, U.S. Naval Civil Eng. Lab., Port Hueneme-CA., 1969.

Nataraja, M.S., Gill, H.S., "Ocean wave-induced liquefaction, J. Geotech. Eng., 109(4), 573-590, 1983.

Sarpakaya, T., "Forces on cylinders near a plane boundary in a sinusoidally oscillating fluid," Trans. ASME J. Fluid Eng., 98, 499-505, 1976.

Verley, R.L. and Reed, K., "Prediction of hydrodynamic forces on seabed pipelines," OTC-5503, 171-180, Houston-TX, April 1987.